Effect of Co, Pd and Pt ultra-thin films on the Ni-silicide formation: Investigating the sandwich configuration

Khalid Quertite*, Jianbao Gao, Marion Descoins, Maxime Bertoglio, Christophe Girardeaux, and Dominique Mangelinck

Aix Marseille Univ, Université de Toulon, CNRS, IM2NP, Marseille, France

* Corresponding author, e-mail: *khalid.quertite@gmail.com*

ABSTRACT

The effect of Co, Pd and Pt ultrathin films on the kinetics of the formation of Ni-silicide by reactive diffusion is investigated. 50nm Ni/1nm X/ 50nm Ni (X=Co, Pd, Pt) deposited on Si(100) substrates are studied using *in-situ* and *ex-situ* measurements by X-ray diffraction (XRD). The presence of Co, Pd or Pt thin films in between the Ni layers delays the formation of the metal rich phase compared to the pure Ni/Si system and thus these films act as diffusion barriers. A simultaneous silicide formation (δ-Ni_2Si and NiSi phases) different from the classic sequential formation is found during the consumption of the top Ni layer for which Ni has to diffuse through the barrier. A model for the simultaneous growth in the presence of a barrier is developed and simulation of the kinetics measured by XRD are used to determine the permeability of the different barriers. Atom probe tomography (APT) of the Ni/Pd/Ni system shows that the Pd layer is located between the Ni top layer and δ-Ni_2Si during the silicide growth, in accordance with a silicide formation controlled by Ni diffusion through the Pd layer. The effect of the barrier on the silicide formation and properties is discussed.

Introduction

With the downscaling of microelectronic devices, NiSi has become the preferred contact material in complementary-metal-oxide-semiconductor (CMOS) transistors [1,2]. Compared to the former metal silicides such as $TiSi_2$ and $CoSi_2$, the NiSi mono-silicide is seen as a more improved intermetallic compound due to its low resistivity and less Si consumption [3,4]. However, NiSi suffers from two degradation mechanisms. Indeed, NiSi start to agglomerate at an intermediate temperature (500°C-700°C). Furthermore, above 750°C, the high resistivity $NiSi_2$ phase starts usually to grow. These two mechanisms present morphological and

thermodynamic challenges that lead to degradation of the contact resistivity. In this context, an extensive work has been done the last two decades in order to improve the Ni-silicide contact performance. Mangelinck et al. [5,6] have reported that the addition of a small amount of Pt alloying element in the Ni layer can delay the agglomeration and increase the $NiSi_2$ formation temperature that usually occurs for pure Ni at relatively high temperature (above 600°C for agglomeration depending on the film thickness and around 800°C for $NiSi_2$ formation). Lavoie et al. [7] have investigated the effect of 24 elements alloyed within the Ni film including Co, Pd and Pt. They reported that the Ni silicide stability could be improved, especially with alloying elements such Pd, Pt, W, Rh, Mo and Ta. Other methods have been used to introduce the alloying element such as interlayer, capping layer or sandwich configuration [8–10]. However the alloying elements can also modify the formation of the Ni silicides depending on the methods used to introduce them [11]. Therefore, it is important to study the effect of Co, Pd and Pt thin films on the nickel silicide formation in the different configuration including the sandwich one.

The growth of Ni silicides in thin films involves reactive diffusion in which both diffusion and reaction contribute [12,13]. The growth is characterized by a sequential formation and sometimes by the growth of transient phases and/or metastable phases [14–16]. It was shown that after the nucleation and lateral growth that result in a continuous film, the thickening of the film takes place following a linear-parabolic growth that can be described by the model of Deal and Grove [17]. Previous works show that adding alloy elements to a Ni film can alter the sequence formation of Ni silicide. For example, for Ni(10 to 13 at. % Pt), the metastable phase $\theta - Ni_2Si$ was observed as the first silicide phase [18,19]. For 10 at. % Pd added to Ni film, a homogeneous $Ni_{1-x}Pd_xSi$ solid solution is formed [20]. In this context, the comparison of the two additive structures (alloy and sandwich) can provide a better understanding of the silicide properties from a structural point of view.

In a previous work by Mangelinck et al. [21], the effect of diffusion barrier on the Ni silicide formation was investigated by *in-situ* X-ray diffraction. Two types of diffusion barriers were studied: (i) a thin layer of W deposited between a Ni film and a Si substrate and (ii) Ni alloy films, Ni(1%W) and Ni(5%Pt), that form a diffusion barrier during the reaction with the Si substrate. The kinetics slowdown induced by the barrier were compared and simulated for both types of barrier. In the case of the deposited barrier, a linear parabolic growth is found for the formation of the silicide, with the linear growth contribution increasing with increasing barrier thickness. In contrast, the growth is mainly parabolic for the barrier formed by the reaction

between an alloy film and the substrate. The permeabilities of the two types of barrier were determined and discussed. The developed models fit well with the experiments, leading to a better understanding of the barrier effect on the reactive diffusion. More recently, the effect of a Ti diffusion barrier on the Co silicide formation was also investigated [22].

The goal of this work is to investigate the effect of a diffusion barrier deposited between two Ni layers on the reactive diffusion and more precisely on the kinetics of formation. The kinetics of silicide formation has been measured by *in-situ* X-ray diffraction during steps and isothermal heat treatment of a pure Ni film, or sandwich layers, Ni/X/Ni with (X=Co, Pd, Pt). The use of the sandwich layers is of particular interest to study the barrier effect since they allow within the same sample to measure the kinetics of formation without barrier (first Ni layer directly in contact with Si) and with barrier (second Ni layer at the sample surface). Simulation of the experimental XRD data is used to quantify the change in kinetics in the presence of a deposited barrier and to determine the permeability of the barrier. Atom probe tomography (APT) allows characterizing the distribution of the barrier element.

Materials and Methods

Four types of samples were deposited by magnetron sputtering on Si(100) at room temperature with a base pressure of 10^{-8} Torr by magnetron sputtering using Ni, Co, Pd and Pt targets. Prior to deposition, the Si(100) surface was immersed into a 5% dilute HF solution for 1 min to remove the native oxide. The first sample is a 100 nm thick pure Ni film deposited on the Si surface. The three other samples are two 50 nm thick Ni films deposited on Si and separated with a 1nm thick layer of X barrier where X = Co, Pt, or Pd. In order to prevent sample oxidation during the *in-situ* XRD experiment, a 20 nm thick SiO_2 film was deposited at room temperature on top of all the studied samples. The *in-situ* XRD measurements were performed under a vacuum of 10^{-5} Torr using two heat treatment procedures. For step annealing, the temperature was first increased from room temperature to 150 °C at a rate of 35 °C/min. Then from 150 °C to 400 °C, the temperature was increased by steps of 5 °C, and a 4.3 min long XRD scan was then recorded at a constant temperature. The heating rate between two steps was 10 °C/min. For isothermal annealing, the temperature was increased from room temperature to a given temperature (290 or 300°C) at a rate of 35 °C/min, and 4.3 min-XRD scans were performed successively.

For the APT experiments, needle-shaped samples were prepared using focused ion beam (FIB) system equipped with a micromanipulator. Prior to FIB process, the studied samples were covered with a 100 nm Ni protection layer deposited by physical vapor deposition (PVD) to prevent Ga contamination during the preparation. Further detailed steps were given elsewhere [23] [17]. The APT analyses were performed in a LEAP 3000X HR instrument under the following conditions: voltage mode at 50K, 20% pulse fraction and 0.2% detection rate, and a pressure of 10^{-11} torr. The 3D volume reconstruction was performed with the IVAS software [24][18, 19]. Considering that the behavior of Pt and Pd is highly comparable and that the addition of Pt element in Ni silicide is relatively well understood and have been studied heavily in literature, the APT results presented in this work will focus on the additional Pd layer in the Ni silicide system.

Results

XRD results

Fig. 1 shows the 2θ diffraction angle for four types of sample deposited on Si(100) as a function of temperature (*in-situ* step annealing from 150 to 400°C) : (a) pure 100nm Ni, (b) 50nm Ni/1nm Co/50nm Ni, (c) 50nm Ni/1nm Pd/50nm Ni, and (d) 50nm Ni/1nm Pt/50nm Ni deposited on Si(100) during *in-situ* step annealing from 150 to 400°C. These XRD experiments were performed in order to identify and compare the formation sequences of the Ni silicide for the four samples. For the pure Ni (reference sample), the classic phase formation sequence is confirmed, in which, only the Ni(111) peak is found at the beginning (from 150°C) at around 44.5°. From 200°C, two peaks start to appear at 45.3° and 48.5°, these peaks correspond to the $\delta - Ni_2Si$ phase with the (211) and (020) planes, respectively. The δ phase represented by these two XRD peaks remains until 365°C but the intensity of these peaks decreases due to the transient formation of the $\theta - Ni_2Si$ phase between 230 and 280°C. Finally, following the total consumption of Ni at 315°C, the NiSi phase starts to nucleate and grows by consuming the $\delta - Ni_2Si$ phase. At 400°C, only the NiSi phase exists. This formation sequence will now be compared to the ones of the other samples. The beginning of the phase formation is the same for all the samples with the appearance of the $\delta - Ni_2Si$ at 200°C and the transient formation of the $\theta - Ni_2Si$ between 230 and 280°C. This similarity can be readily understood since the first 50nm Ni layer is in direct contact with the Si substrate and should thus behave as a pure Ni layer. However, in Fig. 1, three main differences can be observed: i) for the three sandwich

samples, the NiSi phase (peak NiSi (020) and NiSi(102)) starts to grow before the total consumption of Ni (peak Ni(111)). ii) The insertion of a thin layer with another element does increase the temperature needed to fully consume the 100nm of Ni. The required temperature for the Ni_2Si phase complete formation is also increased. In details, the total consumption of Ni is found to occur around 335°C, 370°C, and 360°C for the Ni/X/Ni samples with X = Co, Pd, and Pt, respectively, compared to 315°C for pure Ni. iii) The formation of NiSi is also delayed and the Ni_2Si phase is fully consumed at around 375°C, 395°C, and 385°C for the Ni/X/Ni samples with X = Co, Pd, and Pt, respectively, compared to 365°C for pure Ni. These three differences reveal a diffusion barrier effect for the three studied metal layers, especially for the case of Pd and Pt. Apart from these differences, no major changes such as a shift in the diffraction angle has been observed. However, all the samples show a small peak shift for the peaks located at 45.3° and 48.5° related to the stress relaxation of the $\delta - Ni_2Si$ phase [25,26] [20, 21].

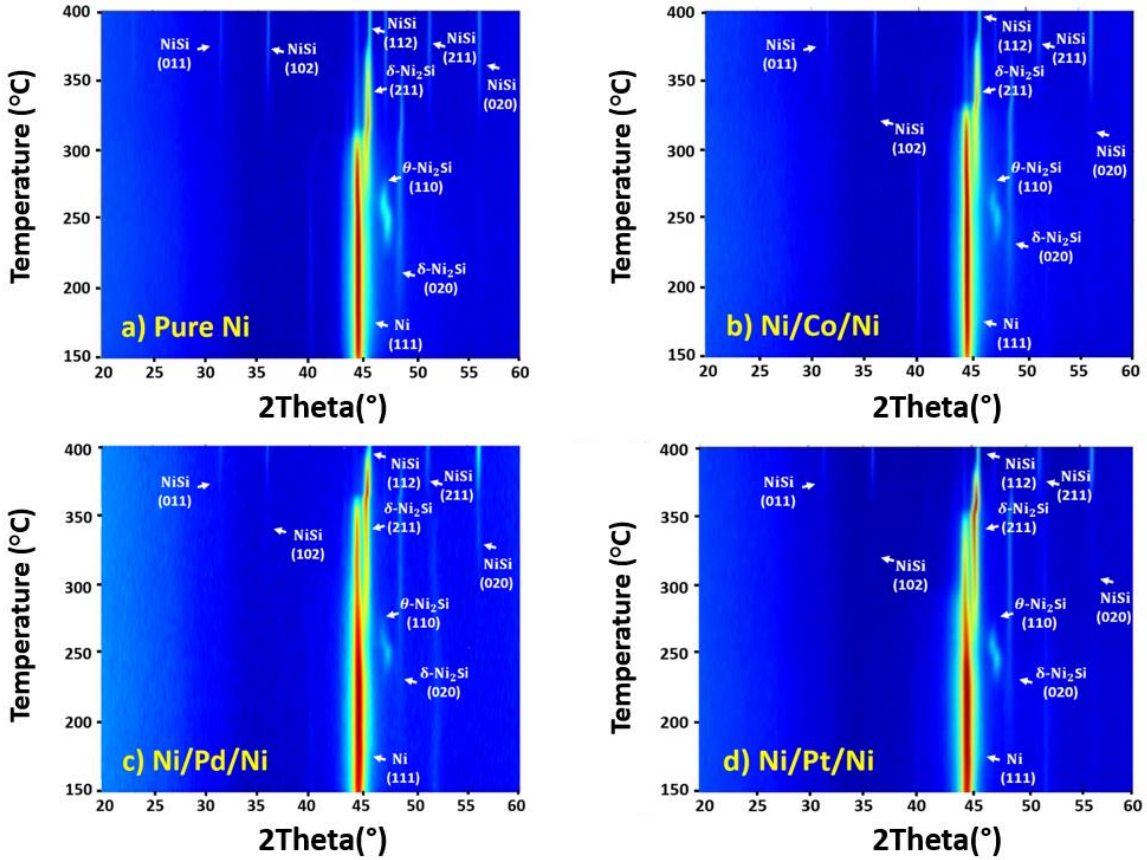

Figure 1 XRD measurements from 150 to 400°C for (a) 100 Ni, (b) 50nm Ni/1nm Co/50nm Ni, (c) 50nm Ni/1nm Pd/50nm Ni, and (d) 50nm Ni/1nm Pt/50nm Ni deposited on Si(100) during *in-situ* step annealing.

Fig. 2 and Fig. 3 show *in-situ* XRD measurements performed during isothermal annealing at 290 and 300°C for a) pure 100nm Ni, (b) 50nm Ni/1nm Co/50nm Ni, (c) 50nm Ni/1nm Pd/50nm Ni, and (d) 50nm Ni/1nm Pt/50nm Ni deposited on Si(100). These XRD data are in accordance with the results described above showing that the insertion of a thin layer of Co, Pd or Pt does delay the consumption of Ni. The XRD data show that in order to consume the deposited 100nm of Ni during heat treatment at 290°C the following durations are required: 200 min, 770 min, and 620 min for the Ni/X/Ni samples with X = Co, Pd, and Pt, respectively, compared to 100 min for pure Ni. For the 300°C isotherm heat treatment, these durations are : 150 min, 400 min, and 375 min for Co, Pd, and Pt layers, respectively, compared to 75 min for pure Ni. In addition, the presence of these layers does modify the Ni silicide phase sequence by leading to the growth of the NiSi phase (e.g., the NiSi peak at 56°) before the total consumption of metal film.

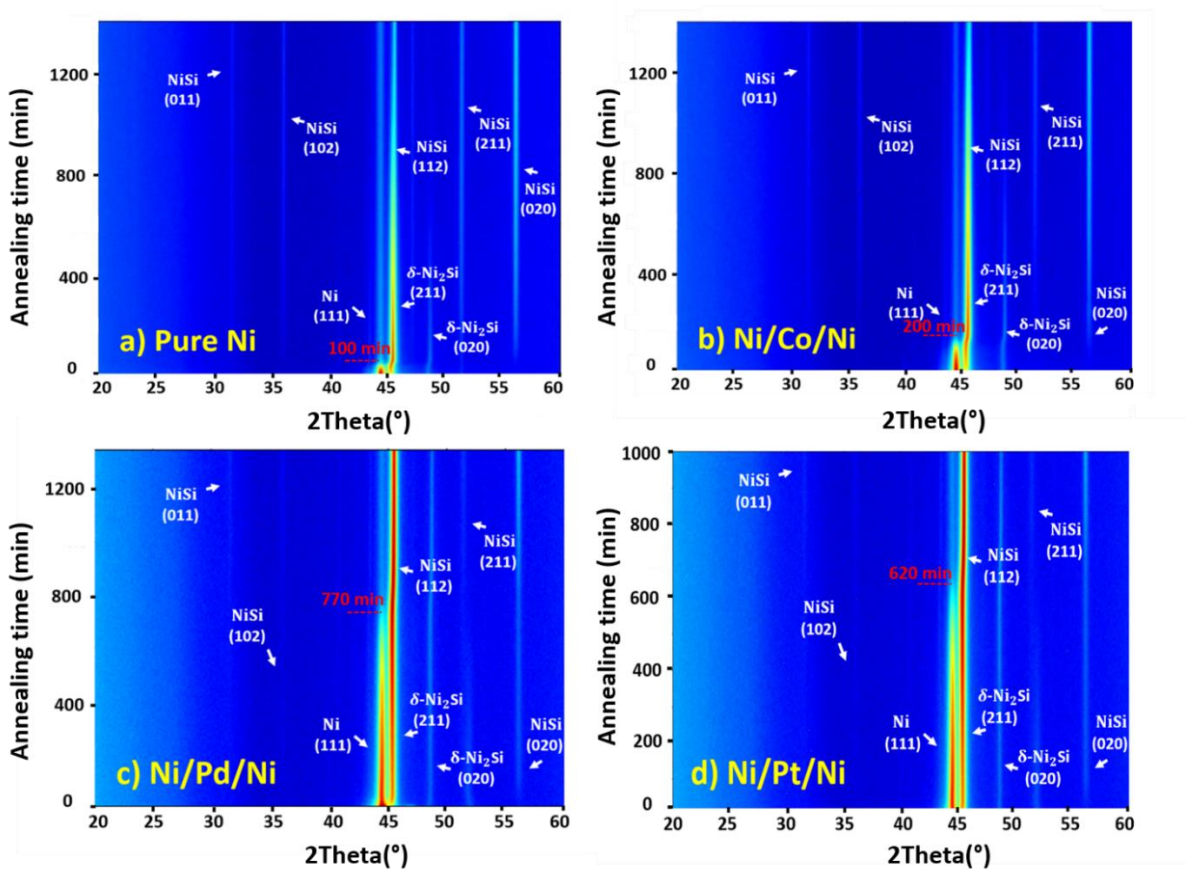

Figure 2 *In-situ* XRD measurements at 290°C for (a) 100 Ni, (b) 50nm Ni/1nm Co/50nm Ni, (c) 50nm Ni/1nm Pd/50nm Ni, and (d) 50nm Ni/1nm Pt/50nm Ni deposited on Si(100). Note that the time scale is not the same for all the measurements.

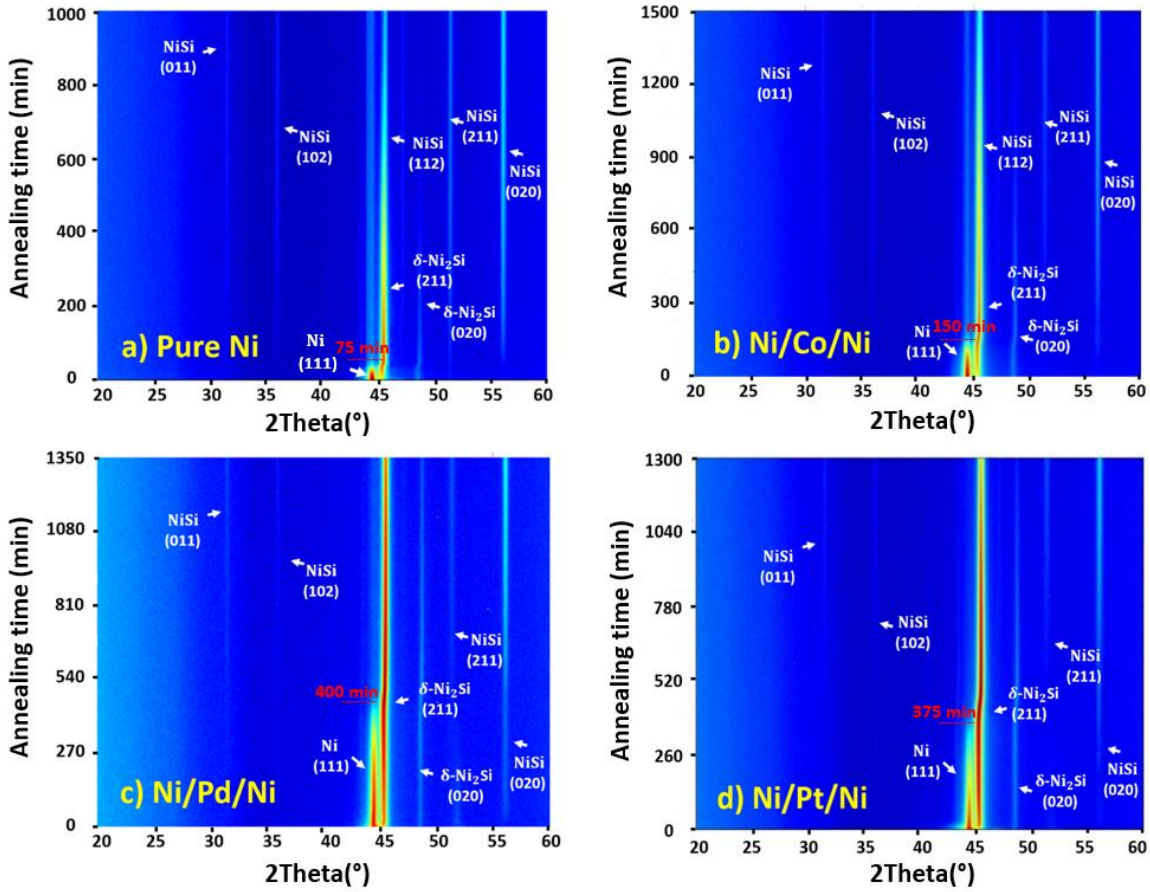

Figure 3 *In-situ* XRD measurements at 300°C for (a) 100 Ni, (b) 50nm Ni/1nm Co/50nm Ni, (c) 50nm Ni/1nm Pd/50nm Ni, and (d) 50nm Ni/1nm Pt/50nm Ni deposited on Si(100). Note that the time scale is not the same for all the measurements.

APT Results

Fig. 4 shows APT reconstructions of the Ni/Pd/Ni sample in the as deposited state and after annealing up to 340 °C. For each APT reconstruction, each dot represents an atom and different colors are used to recognize different elements: Ni in green, Pd in blue and Si in red. The corresponding one-dimensional (1-D) concentration profiles are taken along the z direction perpendicular to the silicide/substrate interface by integrating the number of atoms that exists in a considered volume inside a cylinder (with the same diameter for all the studied volumes). Due to the relatively large thickness of the layers in these two samples and the difficulty to analyze large volume by APT (FIB preparation, tip fracture…), only part of the layers within a given sample are present in Fig. 4. For the as deposited sample, the two Ni layers and the barrier can be seen in Fig. 4.a while only the bottom Ni layer and the Si substrate are present in Fig. 4.b. Similarly, only the top, medium and bottom parts of the layers for the annealed sample are

present in Fig. 4.c, 4.d, and 4.e respectively. For better visibility, Fig. 5.a and Fig. 5.b show a superposition of these APT volumes. The corresponding *ex-situ* XRD is presented in Fig. 5.e and it shows for the as deposited sample a single peak at 44.5° corresponding to the Ni(111) peak. From the APT results in Fig. 4 ~~5.a~~ and Fig. 5~~.c~~, the sandwich structure is verified, showing the Pd film in between two layers of Ni. After annealing the sample at 340°C, the *ex-situ* XRD measurement reveals that the initial Ni peak has been reduced up to 85%, which means that only a small amount of the metal remains on the surface. The most intense peak at 45.3° corresponds to the $\delta - Ni_2Si$ and the less intense peak at 56° presents the NiSi phase. The APT volume in Fig. 5.b validates the XRD showing two kinds of silicide. The one-dimensional concentration profile shows that the thicker silicide with a content of Ni (~67%) two times higher than Si (~33%) corresponds to the $\delta - Ni_2Si$ phase, while, the second silicide with equal content of Ni and Si corresponds to the NiSi phase. In addition, both experiments (XRD and APT) confirm the absence of the meta-stable phase $\theta - Ni_2Si$. For the annealed sample (Fig. 5.b), the main part of Pd atoms is found as a Pd rich layer between the unreacted Ni and the $\delta - Ni_2Si$ phase. This means that the deposited layer is still present and can act as a barrier for the diffusion of Ni atoms. Fig. 5.d shows the corresponding concentration profile, Pd is also present at the grain boundary (GB) of δ-Ni_2Si and a small Pd accumulation is observed close to the δ-Ni_2Si/NiSi interface. Very low concentration of Pd is found in the NiSi phase (<1%). It is important to note that, in the Pd-rich region, the full width at half maximum (FWHM) of the Pd peak has changed during the growth of the δ-Ni_2Si phase from the initial state. Indeed, at 340°C a widening of the Pd-rich region is observed, the FWHM of the Pd peak increased from 2 to 4 nm and the maximum Pd concentration decreased from 38% to 18%. This could suggest that a Pd diffusion has occurred during the growth of δ-Ni_2Si. The diffusion of an impurity in a polycrystalline film such as Pd in δ-Ni_2Si layer depends on the diffusion coefficients at GB and in the grains but also to the segregation of the impurity at GB [15]. The determination of the diffusion coefficients needs a dedicated study with numerous heat treatments that is beyond the scoop of this work but the APT measurements performed on the sample annealed at 340°C allows to quantify the segregation of Pd at the δ-Ni_2Si GB as shown in Fig. 6. For this quantification, cumulative profiles were performed using two cylinders with 10 nm diameter placed perpendicularly to two grain boundaries highlighted by an isoconcentration of 1.5 at% Pd (Fig. 6.a). Accordingly to the standard method [27], the cumulative profiles allows to determine the amount of Pd atoms located at the GB (red vertical bar in Fig. 6.b and 6.c) and to calculate the excess from the cylinder diameter. Two different values were obtained for the two GBs (3.9 and 10 at/nm^2) and they are in the same range than the values obtained for Ti

segregation at the $CoSi_2$ GBs [28,29]. Their differences could be explained by different structures of the GB [28]. Furthermore, the grain size of δ-Ni_2Si can be estimated from Fig. 6.a to be around 10 nm in accordance with SEM/EBSD measurements (not shown here).

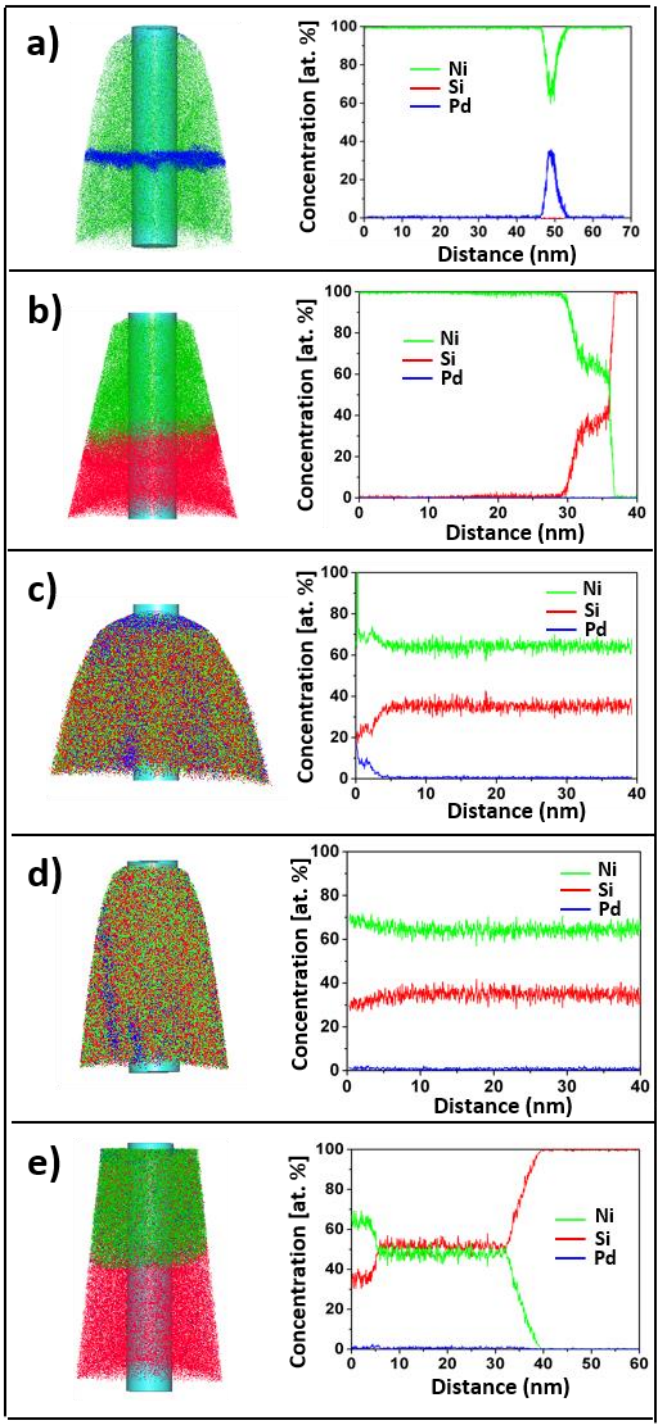

Figure 4 APT analysis for 50nm Ni/1nm Pd/50nm Ni/Si(100) : (a), (b) after deposition at room temperature; (c)-(e) after annealing at 340°C in a vacuum chamber. In the reconstructed volumes (left parts of the figure), each dot represents an atom and different colors are used to

recognize different elements: Ni in green, Pd in blue and Si in red. The one-dimensional (1D) concentration profiles (right parts of the figure) corresponding the reconstructed volume are taken along the z direction perpendicular to the silicide/substrate interface by counting the number of atoms within given thickness slices of a cylinder (with the same diameter for all the studied volumes).

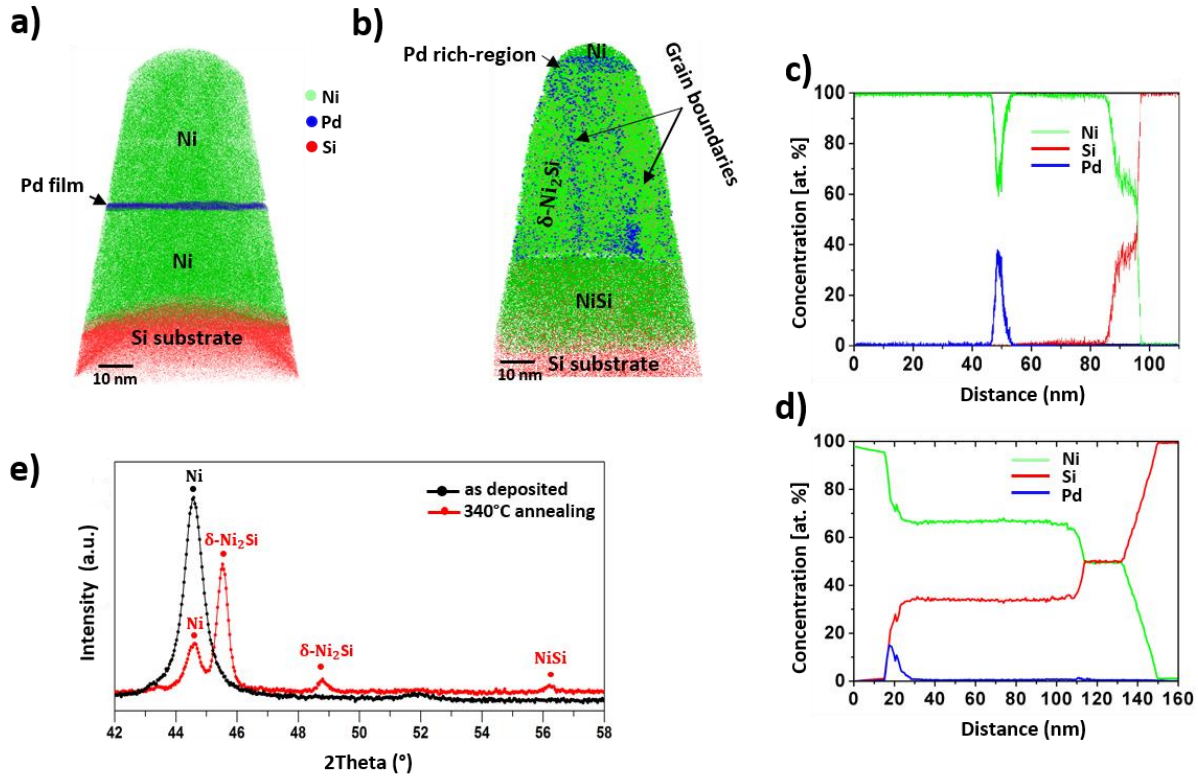

Figure 5 (a) APT volume for 50nm Ni/1nm Pd/50nm Ni/Si(100) after deposition (b) APT volume for 50nm Ni/1nm Pd/50nm Ni/Si(100) after annealing at 340°C in a vacuum chamber. (c) and (d) are the corresponding 1D concentration profiles of (a) and (b), respectively. (e) Shows an *ex-situ* XRD scan of the studied systems, where the black and red dotted lines present (a) and (b) samples, respectively. We note that the APT volumes presented here are a superposition of multiple APT volumes taking from the same experiment and with the same sample.

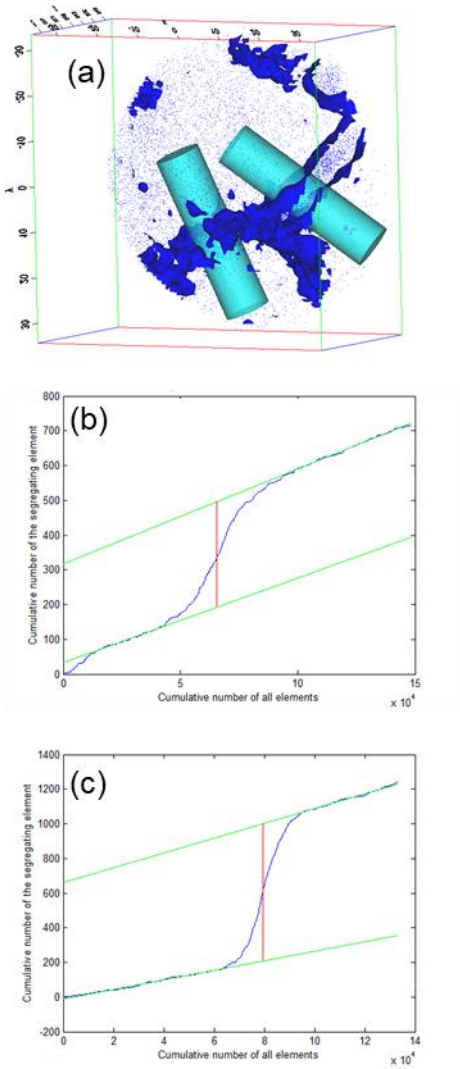

Figure 6: Quantification of the Pd segregation at the δ-Ni_2Si GBs by APT: (a) part of the volume shown in Fig. 4.d in which only the Pd atoms are shown (dark blue points) with an isoconcentration at 1.5 at.% of Pd (dark blue surfaces) together with the two cylinders (light blue color) used to determine the cumulative concentration profiles in (b) and (c). The red vertical bars in (b) and (c) correspond to the number of Pd atoms located at the δ-Ni_2Si GB.

Discussion

Kinetics of Silicide Formation

The *in-situ* XRD experiments (Fig. 1-3) show that the presence of a barrier layer changes the kinetics of formation of the nickel silicide. As no change in the texture (i.e., no change in the ratio between the XRD peak intensities) is observed for the different phases, the experimental XRD intensity should be proportional to the volume of a given phase, which is related to its

thickness since the sample surface is constant. Therefore, by fitting the intensity peaks with a pseudo-Voight function, followed by a normalization and a multiplication by the expected thickness of each silicide phase (that is proportional to the Ni thickness and the ratio of the atomic volumes of the phases), the measured XRD intensities were converted into thicknesses. Fig. 7 presents the thicknesses as a function of the temperature for the studied systems: the first part of the formation of the metal rich phase (i.e., for about half the final thickness of δ-Ni_2Si) is similar for all the systems. However, the second part of the formation is delayed in the presence of additional layers of Co, Pd, and Pt. Indeed, the full formation for the δ-Ni_2Si phase happens at 335°C, 370°C, and 360°C for the Ni/X/Ni samples with X=Co, Pd, and Pt, respectively, compared to 315°C for pure Ni. Among these barrier elements, Pd is thus the most efficient to slow down the metal consumption followed by Pt and Co. This order in the efficiency of Pd, Pt and Co was confirmed by the in situ isothermal annealing at 290 and 300°C in which increasing times are needed to complete the consumption of Ni. Furthermore, our results show the simultaneous presence of the δ-Ni_2Si and NiSi phases while the Ni film is still present during the second part of the formation for the samples with the Co, Pd, and Pt thin layers. This behavior is due to the sandwich structure of the samples, in which, the bottom layer of Ni is in direct contact with the Si substrate while the top Ni layer is separated by the barrier layer. The kinetics of formation of δ-Ni_2Si is thus similar to the pure Ni case for the bottom layer (first part of formation) while the diffusion of Ni through the additional layer (Co, Pd, or Pt) is limited during the consumption of the top layer (second part of the growth) and thus slows down the growth of δ-Ni_2Si. This leads also to the formation of NiSi phase together with δ-Ni_2Si while the Ni top layer is still in the process of consumption. The APT results for the Ni/Pd/Ni sample annealed until 340°C during a step annealing confirm the simultaneous growth of δ-Ni_2Si and NiSi observed by *in-situ* XRD. This behavior is different from the sequential growth observed for the pure Ni but a similar simultaneous growth has been reported for Ni films alloyed with different elements [7] including Au [30], Pt [31] and Pd [26]. A more complex sequence of formation has been also observed for the (Pt+W) alloying elements in the W rich region with a reverse phase formation in which the NiSi phase starts to grow at a temperature lower than that of the δ-Ni_2Si one [32].

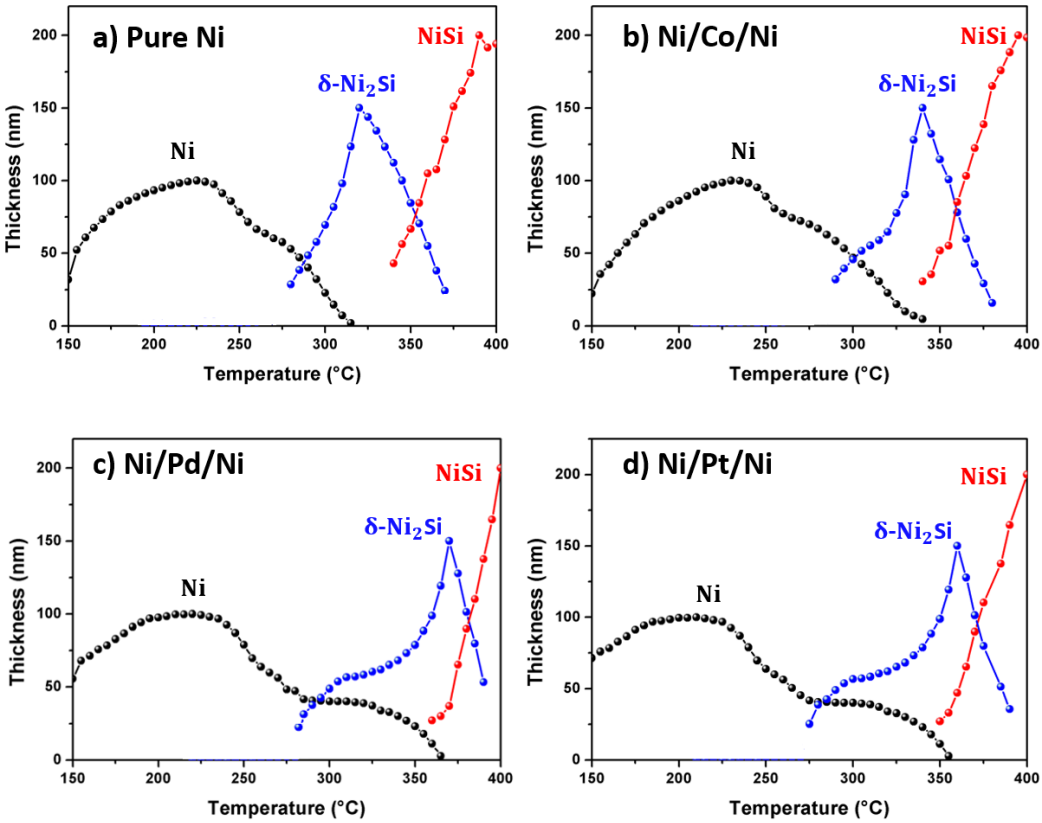

Figure 7 Thickness as a function of temperature for (a) 100 Ni, (b) 50nm Ni/1nm Co/50nm Ni, (c) 50nm Ni/1nm Pd/50nm Ni, and (d) 50nm Ni/1nm Pt/50nm Ni deposited on Si(100) during in situ annealing from 150 to 400 °C.

In order to compare the kinetics of formation for the different samples, a model based on the framework of Mangelinck et al. [21] is now developed to take into account the observed simultaneous growth of and NiSi. The schematic diagram in Fig. 8 illustrates this situation in which two phases ($\delta = A_pB_q$ and $\eta = A_rB_s$) are growing between the two ends members (pure elements), α = A and γ = B, in the presence of a diffusion barrier β. We assume that the atom A is the main diffusing specie (i.e., Ni atoms diffuse much faster than Si atoms in δ-Ni_2Si and NiSi) and that the diffusion of B atom is negligible in all the phases.

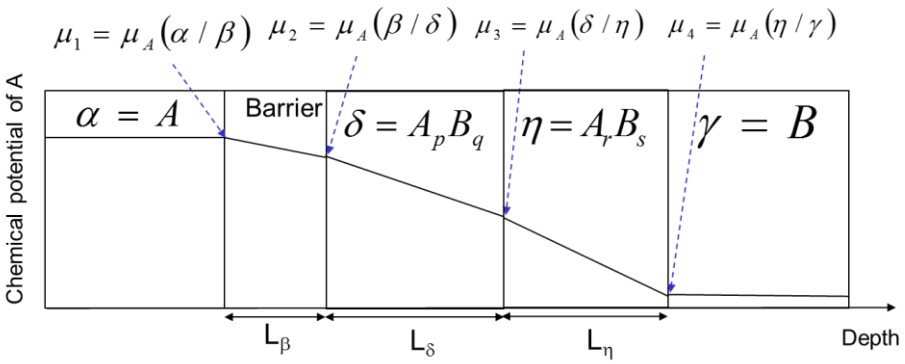

Figure 8 Schematic diagram of the growth of Ni_2Si (δ) and NiSi (η) phases in the presence of a barrier layer (β). Ni film and Si substrate are presented by (α) and (γ), respectively.

In this case, the growth rates of the δ and η phases are given by :

$$\frac{dL^{\delta}}{dt} = a^{\delta\delta} J^{\delta} - a^{\delta\eta} J^{\eta} \tag{1}$$

$$\frac{dL^{\eta}}{dt} = -a^{\eta\delta} J^{\delta} + a^{\eta\eta} J^{\eta} \tag{2}$$

where (L^{δ}, L^{η}) and (J^{δ}, J^{η}) are the thickness and the flux of A through the phases (δ, η). The coefficients $a^{\delta\delta}$, $a^{\eta\eta}$, $a^{\delta\eta}$ and $a^{\eta\delta}$ are positives and are given by :

$$a^{\delta\delta} = \frac{s}{d}\Omega^{\delta}; a^{\delta\eta} = a^{\delta\delta} = \frac{s}{d}\Omega^{\delta} \tag{3}$$

$$a^{\eta\delta} = \frac{q}{d}\Omega^{\eta}; a^{\eta\eta} = \left(\frac{q}{d} + \frac{1}{r}\right)\Omega^{\eta} \tag{4}$$

Where $d = sp - qr$. Ω^{δ} and Ω^{η} are the volumes of the phases δ and η.

$$\Omega^{\varphi} = (p+q)\omega^{\varphi} = \frac{\omega^{\varphi}}{x^{\varphi}} = \frac{1}{c_A^{\varphi}} \tag{5}$$

Ω^{φ} , ω^{φ} , x^{φ} ,and c_A^{φ} are, respectively, the volume occupied by a formula unit, the atomic volume, the atomic fraction and the concentration of the diffusing species.

As shown previously [13,14,21], the flux through a phase can be expressed as:

$$J^{\varphi} = \frac{c_A^{\varphi} \triangle \mu_A^{\varphi}}{RT} \left(\frac{1}{\frac{L^{\varphi}}{D_A^{\varphi}} + \frac{1}{K^{\varphi}}} \right) \tag{6}$$

where φ stands for a phase (δ, η…), D and K are the diffusion and the interfacial reaction coefficients, for the phase φ, and follow an Arrhenius behavior : $D^{\varphi} = D_0^{\varphi} \exp(-\frac{E_D^{\varphi}}{K_B T})$ and $K^{\varphi} = K_0^{\varphi} \exp(-\frac{E_K^{\varphi}}{K_B T})$, $\Delta\mu_A^{\varphi}$ is the chemical potential changes per moving A atom through the phase φ and are given for δ and η by:

$$\Delta\mu_A^{\delta} = \left|\mu_A(\delta/\eta) - \mu_A(\alpha/\delta)\right| \approx \frac{\left(1-x_A^{\delta}\right)G^{\eta} - \left(1-x_A^{\eta}\right)G^{\delta}}{x_A^{\delta} - x_A^{\eta}} \tag{7}$$

$$\Delta\mu_A^{\eta} = \left|\mu_A(\delta/\eta) - \mu_A(\eta/\gamma)\right| \approx \frac{\left(1-x_A^{\delta}\right)G^{\eta} - \left(1-x_A^{\eta}\right)G^{\delta}}{x_A^{\delta} - x_A^{\eta}} - \frac{G^{\eta}}{x_A^{\eta}} \tag{8}$$

where G^{φ} refers to the Gibbs free energy of formation per atoms for the φ phase. Note that the solubility of B in α and of A in γ were assumed to be negligible to establish Eq. 7 and 8.

In the presence of a barrier, the flux of A in δ needs to be modified [21]:

$$J^{\delta} = \frac{c_A^{\delta}\Delta\mu_A^{\delta}}{RT}\left(\frac{1}{\frac{L^{\delta}}{D_A^{\delta}} + \frac{1}{K^{\delta}} + \frac{1}{K^{\beta}}}\right) = \frac{c_A^{\delta}\Delta\mu_A^{\delta}}{RT}\left(\frac{1}{\frac{L^{\delta}}{D_A^{\delta}} + \frac{1}{K^{ef}}}\right) \tag{9}$$

where the effect of the barrier with a fixed thickness and a fixed concentration in A is given by the K^{β} term and can be expressed as:

$$K^{\beta} = \frac{c_A^{\beta} D_A^{\beta}}{c_A^{\delta} L^{\beta}} = \frac{P_A^{\beta}}{x_A^{\delta} L^{\beta}} \tag{10}$$

The permeability of A in the barrier, $P_A^{\beta} = x_A^{\beta} D_A^{\beta}$, reflects the capacity of the barrier to transfer an atom A through the barrier. Note that for the right-hand side expression in Eq. 10, it was assumed that atomic volume is equal in the δ and in β phases.

The effective interface coefficient is defined as :

$$K^{ef} = \left(\frac{1}{K^{\delta}} + \frac{1}{K^{\beta}}\right)^{-1} \tag{11}$$

Eq. 1 to 9 were used to simulate the normalized intensities from the *in-situ* XRD for the second part of the formation (top Ni layer) in the sandwich samples while the first part (bottom Ni layer) for these samples can be fitted by the growth of δ-Ni_2Si alone with the same kinetic parameters than the ones for the pure Ni sample. The simulations and the experiments are presented as a function of the annealing temperature for the step annealing between 150 - 400°C in Fig.9, and as a function of the annealing time for the isothermal heat treatment at 290°C and 300°C in Fig. 10 and Fig. 11, respectively.

As shown in Fig. 9, 10, and 11, the simulated growth behavior of the different phases is in good agreement with the XRD results: for all samples, the first part of the δ-Ni_2Si phase formation which corresponds to the bottom 50 nm Ni layer in direct contact with the Si substrate is similar to the growth from pure Ni and can be fitted with the kinetics parameters of pure Ni sample. For the top Ni layer, the additional layer of Co, Pd or Pt acts as a diffusion barrier, slowing down the diffusion of Ni through it and causing the simultaneous growth of the δ-Ni_2Si and NiSi phases. The main effect of the barrier is to induce a linear growth of the δ-Ni_2Si through the K^{β} term in Eq. 9: this can be clearly seen in Fig. 9 and 10 especially for the Pd and Pt layer. After the complete consumption of Ni, the fast growth of NiSi takes place at the expense of the δ-Ni_2Si phase.

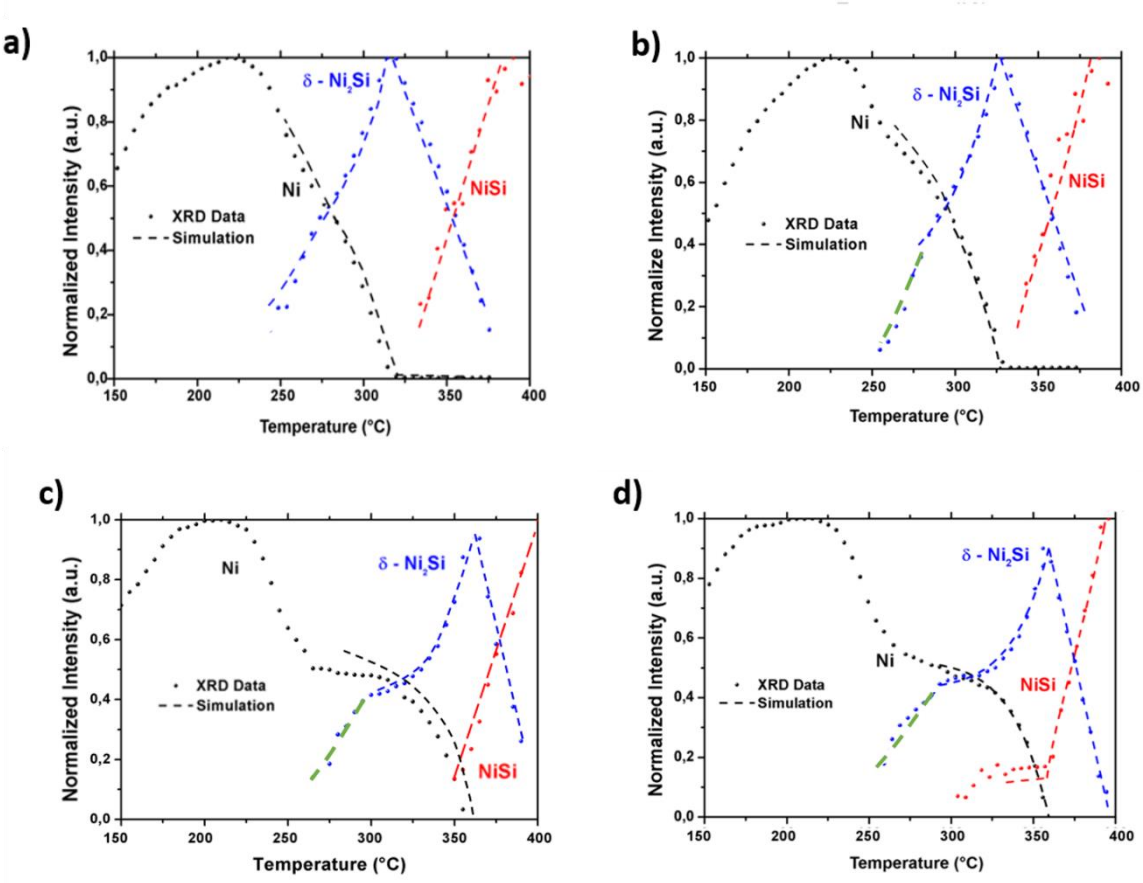

Figure 9 Comparison between XRD and simulation for the kinetics of silicide growth during the *in-situ* step annealing from 150°C-400°C of (a) 100 Ni, (b) 50nm Ni/1nm Co/50nm Ni, (c) 50nm Ni/1nm Pd/50nm Ni, and (d) 50nm Ni/1nm Pt/50nm Ni deposited on Si(100). Black, green, blue, and red dashed lines represent the XRD simulation of the proportion of the Ni, Ni_2Si phases from the bottom Ni layer, δ-Ni_2Si phase from the top Ni layer, and NiSi phase, respectively.

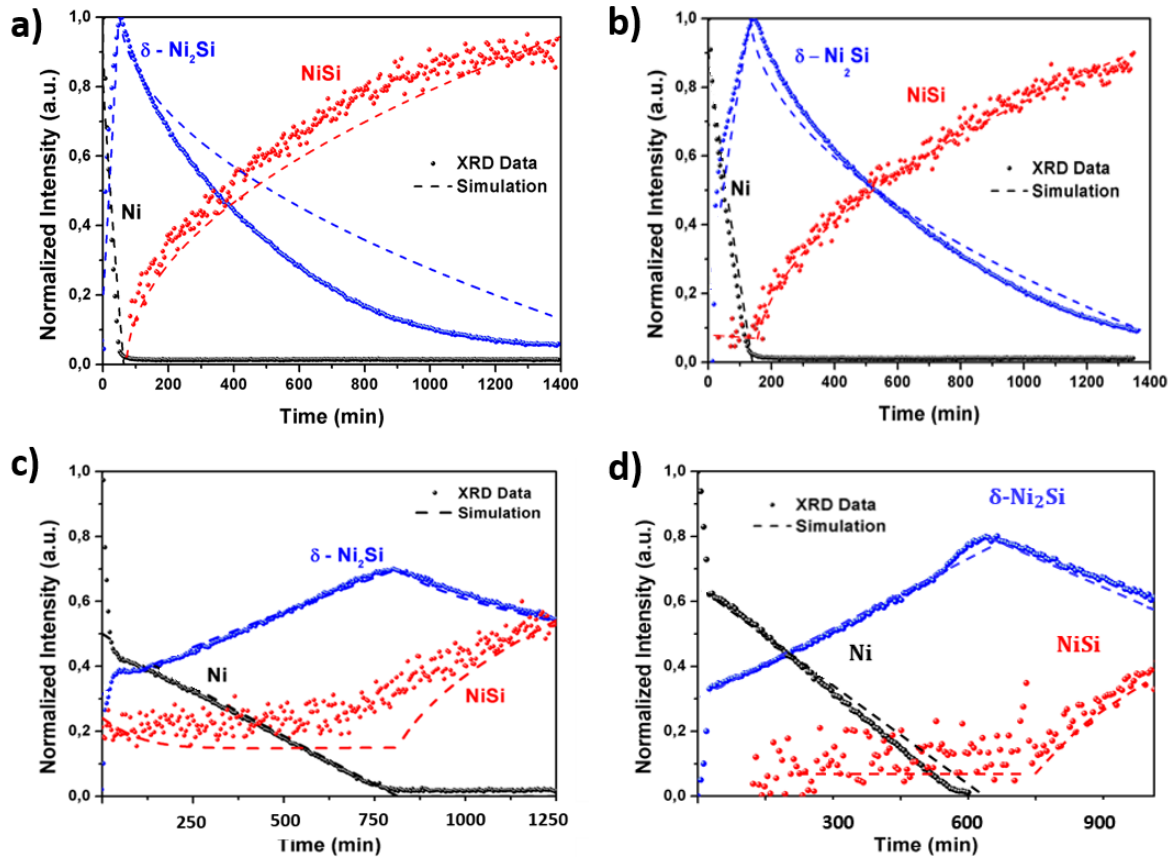

Figure 10 Comparison between XRD and simulation for the kinetics of silicide growth during the in-situ annealing at 290°C of (a) 100 Ni, (b) 50nm Ni/1nm Co/50nm Ni, (c) 50nm Ni/1nm Pd/50nm Ni, and (d) 50nm Ni/1nm Pt/50nm Ni deposited on Si(100). Black, blue, and red dashed lines represent the XRD simulation of the proportion of the Ni, Ni_2Si, and NiSi phases, respectively.

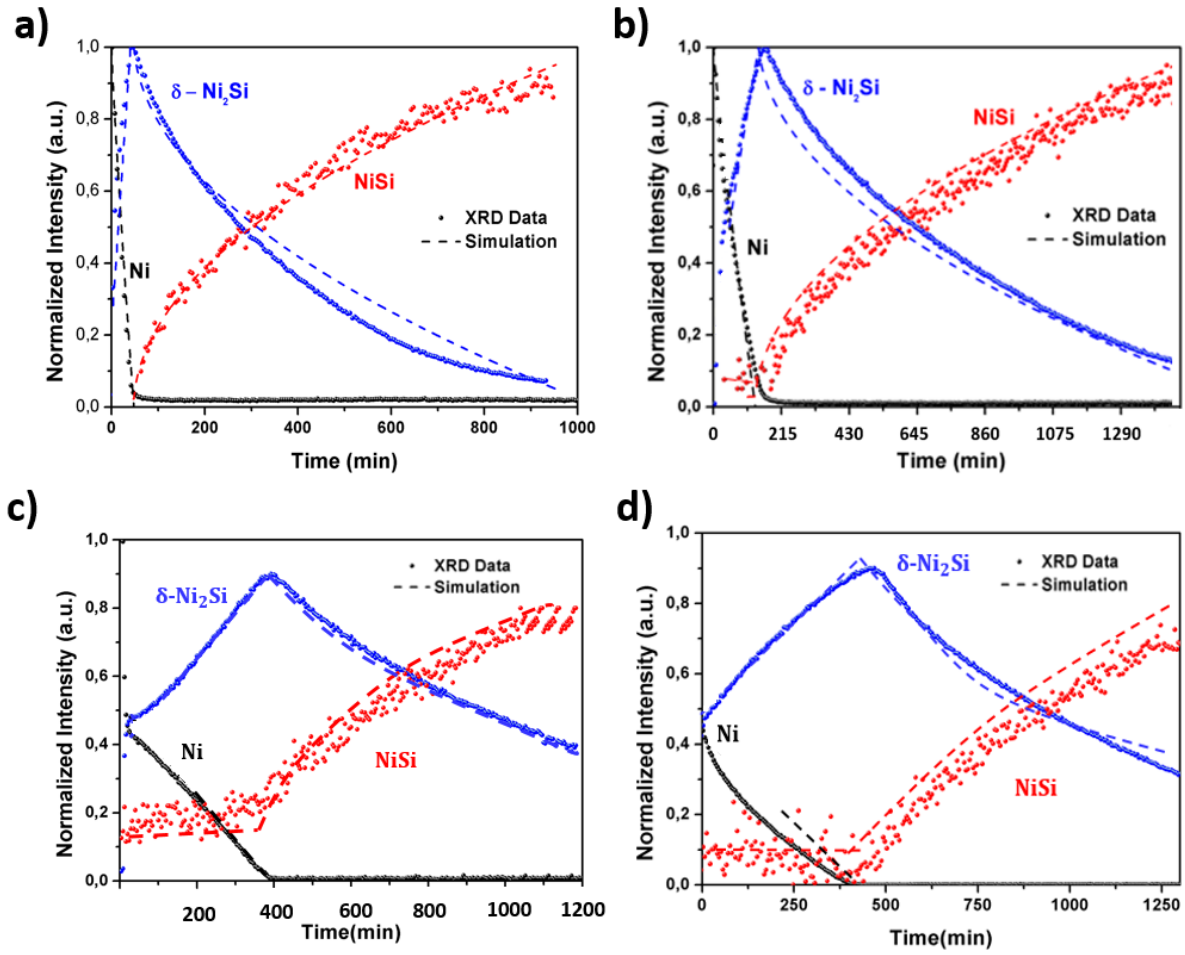

Figure 11 Comparison between XRD and simulation for the kinetics of silicide growth during the in-situ annealing at 300°C of (a) 100 Ni, (b) 50nm Ni/1nm Co/50nm Ni, (c) 50nm Ni/1nm Pd/50nm Ni, and (d) 50nm Ni/1nm Pt/50nm Ni deposited on Si(100). Black, blue, and red dashed lines represent the XRD simulation of the proportion of the Ni, Ni_2Si, and NiSi phases, respectively.

The simulated kinetics parameters such as pre-exponential factors and activation energies of the interface (K) and diffusion (D) coefficients are presented in Table 1. For the pure Ni film, the activation energy is 1.5 eV for $\delta - Ni_2Si$ and 1.6 eV for NiSi. These values are in good agreement with the ones reported in literature [14,33–35]. The activation energies for the interface coefficients for the δ-Ni_2Si phase are 1.40 eV, 1.50 eV, 1.49 eV for the Ni/X/Ni samples with X=Co, Pd, and Pt, respectively, compared to 0.8 eV for pure Ni. The highest energy is obtained for the Pd in accordance with the XRD observations showing that the Pd thin film is more efficient to slow down the complete formation of the δ-Ni_2Si phase.

Table 1 Simulated pre-exponential factors and activation energies of the interface and diffusion coefficients for of Ni, NiCoNi, NiPdNi and NiPtNi systems for δ-Ni_2Si and NiSi phases. Note that the interface coefficient for δ-Ni_2Si corresponds the effective interface coefficient, K^{ef} , for the sandwich samples.

Sample	Phase	$\mathbf{K_0}$ (cm/s)	$\mathbf{E_K}$(eV)	$\mathbf{D_0}$ (cm²/s)	$\boldsymbol{E_D}$(eV)
Ni	δ-Ni_2Si	1	0.8	0.65	1.5
	NiSi	1	0.9	0.25	1.6
Ni/Co/Ni	δ-Ni_2Si	5 x 10^3	1.40	1	1.5
	NiSi	1	0,9	0.08	1.6
Ni/Pd/Ni	δ-Ni_2Si	6 x 10^3	1.50	1	1.5
	NiSi	1	0.9	0.05	1.6
Ni/Pt/Ni	δ-Ni_2Si	6 x 10^3	1.48	1	1.5
	NiSi	1	0.9	0.06	1.6

With these relatively large values of the activation energy, the effective interfacial coefficient, K^{ef}, is much lower than the interface coefficient for δ-Ni_2Si pure Ni (about 50 times for Co, 200 times for Pt and 300 times for Pd at 290°C). If one considers that the interface coefficient for δ-Ni_2Si, K^{δ}, is not changed too much by the presence of the additional layer, this means (Eq. 11) that K^{ef} is almost equal to the barrier coefficient, K^{β}.

From the expression of K^{β} (Eq. 10), it is thus possible to calculate the permeability of the barrier for the δ-Ni_2Si phase, P_A^{β}, from the sandwich sample since x_A^{δ} and L^{β} are known. Table 2 shows that the Pd and Pt thin films have similar permeability (2.6 x 10^{-4} nm²/s and 3.9 x 10^{-4} nm²/s, respectively), in agreement with the XRD results where the growth behavior was similar for the Pd and Pt additional films. On the contrary, the Co thin film has a relatively high permeability (i.e., weakness of the barrier) of 1.6 x 10^{-3} nm²/s almost four times higher than the Pd and Pt films. These permeabilities are on the same range than the ones obtained in Ref. [21] for a W interlayer with a thickness of 0.5 (1.3 x 10^{-4} nm^2/s) or 1 nm (1.0 x 10^{-4} nm^2/s) or for the alloy with 5% Pt (0.9 x 10^{-4} nm^2/s) (note that there was a mistake in Ref. [21] and that the given values were over evaluated by a factor of 100).

One of the advantages of using the sandwich structure is the capability to eliminate some factors that can affect the measured permeability of the barrier. Indeed, it is well known that when a

metal film (e.g., Ni, Co, Pd or Pt) is deposited on Si, an intermixing layer is formed during the deposition. For Ni metal, an intermixing layer of 1 or 3 nm was found [11,36]. In the case of the interlayer structure, an intermixed layer would change the barrier thickness, which could affect the permeability. The intermixed layer consumes part of the interlayer that is directly deposited on the Si substrate. However, if only the metal barrier is efficient as diffusion barrier, the barrier thickness is decreased. On the other hand, if the intermixed layer is also efficient to slow down the diffusion, then the barrier thickness is increased. The permeability in Ref. [21] was determined at 270°C and thus 30°C below the values given below. Using the activation energy for K^{ef} in table 1, the permeability at 270°C for the Pt barrier can be estimated to be 0.7 x 10^{-4} nm^2/s. As this value is lower than the measured one (0.7 x 10^{-4} nm^2/s), the intermixed layer seems to reduce the barrier thickness instead to increase it. However, the Pt permeability was measured from an Ni(Pt) alloy in [21] in which the barrier is built during the formation of the silicide and can thus differs slightly from a barrier with a constant thickness and composition.

It should be mentioned that the model used in our simulation suffers from some limitations. Indeed, the model is based on the one-dimensional growth assumption. However, the formation of silicide is a more complex process in which the mechanisms of nucleation at the interface and lateral growth along the interface should be included. This is especially true for thin films [37]. However, for thicknesses larger than about 10 nm, the nucleation and lateral growth end to a continuous layer, which then maintain a one-dimensional growth mode. Also, the model does not take into account the possibility that the barrier element may change the diffusion in the growing phase by segregating at the grain boundaries as indicated by the APT measurements. The barrier element could also change the interface coefficient, K^{δ}, for example by segregating at the interface. It is thus important to study the distribution of the barrier element. Since the Pt redistribution during the formation of Ni silicides has been relatively well studied [38–40], the redistribution of Pd was studied in this work.

Table 2 Permeability obtained from the fit of the experimental kinetics at T=300°C. Here, $P_{Ni}^{\beta} = K\ x_{Ni}^{\delta} L^{\beta}$ with $x_{Ni}^{\delta} = 2/3$, $L^{\beta} = 1$ nm and K is the calculated reaction coefficient from Table 1.

Sample	P_{Ni}^{β} (nm²/s)
Ni/Co/Ni	1.6 x 10-3
Ni/Pd/Ni	2.6 x 10-4
Ni/Pt/Ni	3.9 x 10-4

Distribution of the Diffusion Barrier Element

The Pd distribution determined by APT after deposition and after annealing at 340°C is shown in Fig. 5. A schematic of the redistribution deduced from these measurements is represented in Fig. 12. After deposition (Fig. 5a), a homogeneous Pd film corresponding to the barrier is obtained and no Pd is found in the Ni layers. As the APT profiling induced some broadening, the concentration of Pd doesn't reach 100% but the integration of the depth profile gives an equivalent thickness of a pure Pd film of 1 nm in accordance with the nominal thickness. After annealing at 340°C (Fig. 5b), a Pd-rich region corresponding to the barrier is observed at the Ni/Ni_2Si interface. This indicates that the barrier layer is preserved during the formation of the Ni silicides. However, the small amount of Pd found in δ-Ni_2Si, located mainly at the grain boundaries (Fig. 5.b), indicates that the barrier thickness should have decreased to some extent. Concerning the location of the barrier at the Ni/δ-Ni_2Si interface (Fig. 5.b), previous work using *in-situ* RBS have shown that during the reaction of Ni(Pd) alloy film with Si, Pd atoms are pushed back in the metal alloy during the growth of the Ni_2Si [26,41]. As a result, a Pd enriched layer is observed between the metal and the silicide and ends at the sample surface when the δ-Ni_2Si formation is finished. This behavior can be due to the low solubility of Pd in the metal rich phase, which is estimated to be around 4% at 800°C [42] and should be lower than this value at the temperatures for which δ-Ni_2Si grows. However, in the case of the sandwich samples, the location of the Pd barrier at the Ni/Ni_2Si interface is more likely due to the fact that Ni is the main diffusing specie during the Ni silicide formation. The Ni atoms cross the barrier to form δ-Ni_2Si leading to a shift of the barrier towards the surface. The faster diffusion of Ni

in the Ni silicides was shown using an implanted noble gas atom as diffusion marker with Rutherford Backscattering Spectrometry (RBS) characterization [12]. In addition, this is in accordance with the "Cu_3Au" rule [43], that states that the metal should be the fastest diffusing species during the formation of metal-rich silicide.

Although the Pd distribution in the sandwich structure (Ni/Pd/Ni/Si) presented in this work (Fig. 12) looks quite similar to the ones reported in in the case of an alloy system (Ni(Pd)/Si) [26,41], still some aspects of the Pd redistribution are different. Our APT results show also that the Pd atoms diffuse through the δ-Ni_2Si silicide mainly at grain boundaries but do not penetrate in the NiSi silicide. Using *in-situ* RBS and XRD coupled with APT measurements, Schrauwen et al. [41] report a complete extrusion of Pd during δ-Ni_2Si growth with the absence of Pd grain boundary decoration in the Ni_2Si silicide. However, our APT results clearly show that Pd atoms are indeed decorating the Ni_2Si grain boundaries in agreement with other work studying the redistribution of Pt during silicide formation, in which, a clear evidence of Pt diffusion short-circuits via δ-Ni_2Si grain boundaries was also observed [44]. This can be of importance because, during Ni silicide formation in thin film, the Ni diffusion occurs mainly via grain boundaries: presence of Pd in the Ni_2Si grain boundaries may slow down the Ni diffusion and, as a result, the silicide formation kinetics will decrease. No major change has been observed for the diffusion coefficient in table 1 but the kinetic of δ-Ni_2Si is mainly controlled by interface term in the presence of the Pd barrier and this change may be difficult to measure.

Furthermore, the observed low content of Pd (<1 at.%) in NiSi phase (Fig. 4.e) may appear odd since NiSi and PdSi share the same crystallographic orthorhombic structure (MnP type, space group: Pnma) with a small lattice parameters mismatch [45], and are thus fully miscible [42]. On the contrary, Schauwen et al. [41] have observed by APT the presence of Pd at the grain boundaries of NiSi. This apparent controversy may be linked to the temperatures where the observations were made. Indeed, in Ref. [41], the absence of GB decoration by Pd in δ-Ni_2Si was observed at about 320°C and the presence of Pd at the NiSi GBs at 500°C: our APT measurement corresponds to an intermediate temperature for which Pd diffusion may be important at the δ-Ni_2Si GBs but very low at the NiSi GBs. This could reflect the importance of grain boundaries as a major factor in the diffusion of Pd in both silicides. The area analyzed by APT being very small, it is also possible that the microstructure of the silicide is different according to the density of the grain boundaries (different grain sizes). Another factor that can affect the silicide kinetics is the segregation of Pd at the δ-Ni_2Si/NiSi interface. Indeed, segregation at this interface may change the interface coefficient. However only a small

segregation has been observed. To conclude, the main effect of the presence of Pd in the sandwich sample appears to be the barrier effect induced by the deposited Pd layer while the effect of Pd segregation/diffusion at GB or interface is less important.

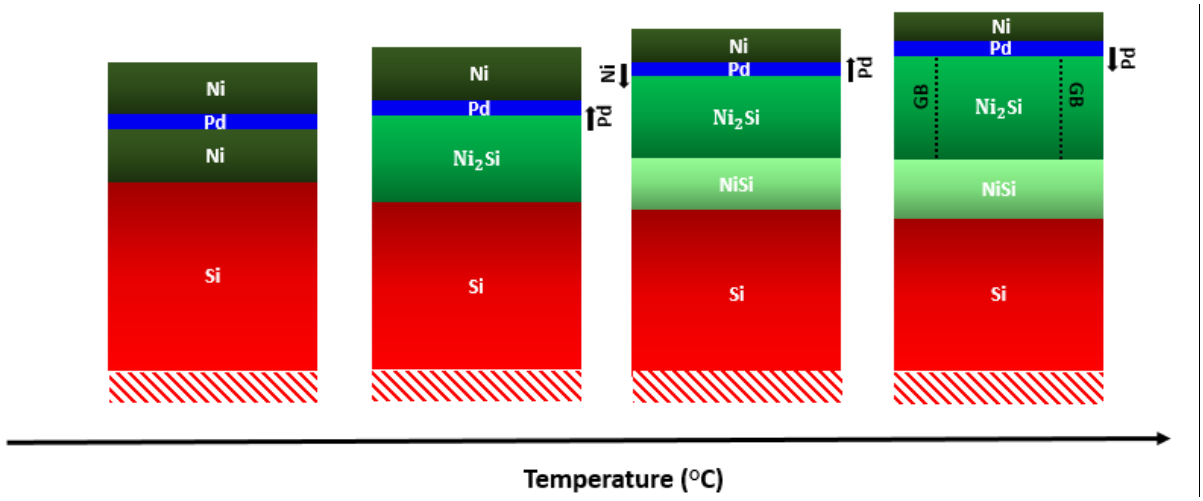

Figure 12 Schematic diagram of the important stages during silicidation of the Ni/Pd/Ni/Si(100) system.

Effect of different diffusion barrier on phase formation and properties

Diffusion barriers are used in numerous applications such as protective coatings in metallurgy, intermetallic control in aeronautics, interlayer in diffusion welding, and contact formation and interconnections in microelectronics. In metallurgy, thin layer of metal are placed between two other metals as diffusion barrier in order to protect one of the metals from modifying the other [46]. In aeronautics, the diffusion barrier may come from the segregation of impurities contained in one of the materials and it could limit the growth of intermetallic [47,48]. In microelectronics, barriers are usually introduced to chemically isolate semiconductors from metal interconnects, while maintaining an electrical connection between them. For instance, a layer of barrier metal must surround every copper interconnection in modern copper-based chips to prevent the diffusion of copper into surrounding materials [49,50]. In several of these cases, the growth of phases such as intermetallics occurs by reactive diffusion.

The presence of a barrier can also change the microstructure and the texture of the growing phase. For example, the presence of a thin layer of Ti or of SiO_2 was found to change the texture of $CoSi_2$ film and in particular to promote the epitaxy of $CoSi_2$ on Si [51,52]. It was also found that changes in texture impact the thermal stability (agglomeration) of silicide thin film [53].

For microelectronics, the incomplete formation of the low resistivity phase (NiSi, $CoSi_2$) induced by the kinetics change in the presence of a barrier may also impact the resistance of the contact since the first growing phase have usually a high resistivity [45]. Unintentional barrier may also arise from impurities due to a partial cleaning before metal deposition and/or to the snowplow of the impurities during the reactive diffusion [38].

For all these applications as well as for the final properties, it is important to understand and control the behavior of the barrier in particular when reactive diffusion is involved. In our former works [21,22], the growth of a single phase in the presence of a diffusion barrier was analyzed. In the case of the growth of δ-Ni_2Si [21], two types of diffusion barriers were studied: (i) a thin layer deposited between the Ni film and a Si substrate and (ii) Ni alloy films in which the alloy element forms a diffusion barrier during the silicide formation because it is not incorporated in the growing silicide (snowplow). In these two cases, there is a slow diffusion through the barrier of the metal (Ni) that is the fast diffusion species in the growing silicide (δ-Ni_2Si). A different case was studied in [22] since the Ti layer is a diffusion barrier for the slow diffusion species (Co) in the growing silicide (CoSi). For these three cases, we have developed models in order to fit the kinetics of phase formation [21,22] and/or the interdiffusion within the metal layer [22]. In the present work, a different case was studied since two phases (δ-Ni_2Si and NiSi) are growing simultaneously due to the sandwich configuration and the developed model allows also a good fit of the kinetics of formation for these two phases. The good accordance between experience and simulation based on these models shows that the barrier can be well described by a single parameter, the permeability that is a product of the diffusion coefficient and the solubility of the diffusing element in the barrier.

The sandwich layers allow not only to measure the kinetics of formation without barrier (first Ni layer directly in contact with Si) and with barrier (second Ni layer at the sample surface) within the same sample but also shows that the position of the barrier is of importance for the formation of silicide: for example, the formation changes from sequential for an interlayer to simultaneous for a sandwich case. This may be used in order to design specific configuration of phases and/or microstructure. The systematic determination of the permeability of various barriers may also to design barrier for different applications. From a more fundamental point of view, the presence of a barrier layer introduces an effective interface coefficient (Eq. 11) that may allow to understand changes in kinetics from parabolic to linear parabolic or even purely linear [39]. This may also contribute to the understanding of the specificities of thin film reaction such as sequential growth, absence of stables phases, growth of metastable phases…

Conclusion

A combined experimental-simulation method has been used to study the effect of a diffusion barrier on the kinetics formation of Ni-silicides~~. This work focuses on~~ using sandwich structures in which an ultra-thin (1 nm) film barrier of either Co, Pd, or Pt is deposited between two 50 nm Ni layers on a Si substrate. The kinetics of formation of δ-Ni_2Si and NiSi have been measured by *in-situ* XRD and the redistribution of Pd by APT ~~for the different samples and compared to the ones of pure Ni (reference sample).~~.

The main conclusions are the following:

- All the studied thin film barriers slow down the Ni silicide formation: a strong barrier effect is obtained for Pd, which is close to Pt and much higher than Co.
- The sandwich samples show simultaneous silicide formation (δ-Ni_2Si and NiSi) different from the classic sequential formation.
- A model for the simultaneous growth of two phases in the presence of a barrier with fixed thickness and fixed concentration has been developed.
- The good accordance between experience and simulation based on this model shows that the barrier can be well described by a single parameter, the permeability (product of the diffusion coefficient and the solubility of the diffusing element in the barrier) that reflects the efficiency of each barrier.
- APT shows that the Pd barrier is located between the Ni and δ-Ni_2Si during the δ-Ni_2Si growth as expected from predominant diffusion of Ni in δ-Ni_2Si.
- The implication of the barrier in terms of silicide formation and properties is discussed.

The combination of experimental results, model and simulation allows to better understand the effect of a barrier on the silicide formation and to predict the barrier behavior at the nanoscale. Thus, it may help us to design barriers for silicide applications in microelectronics as well as for other applications.

Declaration of Competing Interest

The authors declare that they have no conflict of interests or personal relationships that could have appeared to influence the work reported in this paper.

References

[1] C. Lavoie, F.M. d'Heurle, C. Detavernier, C. Cabral Jr., Towards implementation of a nickel silicide process for CMOS technologies, Microelectronic Engineering. 70 (2003) 144–157. https://doi.org/10.1016/S0167-9317(03)00380-0.

[2] F. Deng, R.A. Johnson, P.M. Asbeck, S.S. Lau, W.B. Dubbelday, T. Hsiao, J. Woo, Salicidation process using NiSi and its device application, Journal of Applied Physics. 81 (1997) 8047–8051. https://doi.org/10.1063/1.365410.

[3] H. Iwai, T. Ohguro, S. Ohmi, NiSi Salicide Technology for Scaled CMOS, Microelectron. Eng. 60 (2002) 157–169. https://doi.org/10.1016/S0167-9317(01)00684-0.

[4] J.A. Kittl, A. Lauwers, O. Chamirian, M. Van Dal, A. Akheyar, M. De Potter, R. Lindsay, K. Maex, Ni- and Co-based silicides for advanced CMOS applications, Microelectronic Engineering. 70 (2003) 158–165. https://doi.org/10.1016/S0167-9317(03)00370-8.

[5] D. Mangelinck, J.Y. Dai, J.S. Pan, S.K. Lahiri, Enhancement of thermal stability of NiSi films on (100)Si and (111)Si by Pt addition, Applied Physics Letters. 75 (1999) 1736–1738. https://doi.org/10.1063/1.124803.

[6] D. Mangelinck, J.Y. Dai, S.K. Lahiri, C.S. Ho, T. Osipowicz, Formation and Stability of NI(PT) Silicide on (100)SI and (111)SI, MRS Proceedings. 564 (1999). https://doi.org/10.1557/PROC-564-163.

[7] C. Lavoie, C. Detavernier, C. Cabral, F.M. d'Heurle, A.J. Kellock, J. Jordan-Sweet, J.M.E. Harper, Effects of additive elements on the phase formation and morphological stability of nickel monosilicide films, Microelectronic Engineering. 83 (2006) 2042–2054. https://doi.org/10.1016/j.mee.2006.09.006.

[8] W. Huang, L. Zhang, Y. Gao, H. Jin, Effect of a thin W, Pt, Mo, and Zr interlayer on the thermal stability and electrical characteristics of NiSi, Microelectronic Engineering. 84 (2007) 678–683. https://doi.org/10.1016/j.mee.2006.11.006.

[9] R.N. Wang, J.Y. Feng, Comparison of the thermal stabilities of NiSi films in Ni/Si, Ni/Pd/Si and Ni/Pt/Si systems, J. Phys.: Condens. Matter. 15 (2003) 1935. https://doi.org/10.1088/0953-8984/15/12/310.

[10] J. Demeulemeester, W. Knaepen, D. Smeets, A. Schrauwen, C.M. Comrie, N.P. Barradas, A. Vieira, C. Detavernier, K. Temst, A. Vantomme, In situ study of the growth properties of Ni-rare earth silicides for interlayer and alloy systems on Si(100), Journal of Applied Physics. 111 (2012) 043511. https://doi.org/10.1063/1.3681331.

[11] M. El Kousseifi, K. Hoummada, M. Bertoglio, D. Mangelinck, Selection of the first Ni silicide phase by controlling the Pt incorporation in the intermixed layer, Acta Mater. 106 (2016) 193–198. https://doi.org/10.1016/j.actamat.2016.01.004.

[12] W.K. Chu, S.S. Lau, J.W. Mayer, H. Müller, K.N. Tu, Implanted noble gas atoms as diffusion markers in silicide formation, Thin Solid Films. 25 (1975) 393–402. https://doi.org/10.1016/0040-6090(75)90057-7.

[13] F. Nemouchi, D. Mangelinck, C. Bergman, P. Gas, U. Smith, Differential scanning calorimetry analysis of the linear parabolic growth of nanometric Ni silicide thin films on a Si substrate, Applied Physics Letters. 86 (2005) 041903. https://doi.org/10.1063/1.1852727.

[14] F.M. d'Heurle, P. Gas, Kinetics of formation of silicides: A review, Journal of Materials Research. 1 (1986) 205–221. https://doi.org/10.1557/JMR.1986.0205.

[15] D. Mangelinck, Chapter 9 - The Growth of Silicides and Germanides, in: A. Paul, S. Divinski (Eds.), Handbook of Solid State Diffusion, Volume 2, Elsevier, 2017: pp. 379–446. https://doi.org/10.1016/B978-0-12-804548-0.00009-8.

[16] S. Gaudet, C. Coia, P. Desjardins, C. Lavoie, Metastable phase formation during the reaction of Ni films with Si(001): The role of texture inheritance, Journal of Applied Physics. 107 (2010) 093515. https://doi.org/10.1063/1.3327451.

[17] B.E. Deal, A.S. Grove, General Relationship for the Thermal Oxidation of Silicon, Journal of Applied Physics. 36 (1965) 3770–3778. https://doi.org/10.1063/1.1713945.

[18] M. Putero, L. Ehouarne, E. Ziegler, D. Mangelinck, First silicide formed by reaction of Ni(13%Pt) films with Si(1 0 0): Nature and kinetics by in-situ X-ray reflectivity and diffraction, Scripta Materialia. 63 (2010) 24–27. https://doi.org/10.1016/j.scriptamat.2010.02.040.

[19] F. Panciera, D. Mangelinck, K. Hoummada, M. Texier, M. Bertoglio, A. De Luca, M. Gregoire, M. Juhel, Direct epitaxial growth of θ-Ni2Si by reaction of a thin Ni(10 at.% Pt) film with Si(1 0 0) substrate, Scripta Materialia. 78–79 (2014) 9–12. https://doi.org/10.1016/j.scriptamat.2014.01.010.

[20] A. Schrauwen, J. Demeulemeester, D. Deduytsche, W. Devulder, C. Detavernier, C.M. Comrie, K. Temst, A. Vantomme, Ternary silicide formation from Ni-Pt, Ni-Pd and Pt-Pd alloys on Si(100): Nucleation and solid solubility of the monosilicides, Acta Materialia. 130 (2017) 19–27. https://doi.org/10.1016/j.actamat.2017.03.022.

[21] D. Mangelinck, T. Luo, C. Girardeaux, Reactive diffusion in the presence of a diffusion barrier: Experiment and model, Journal of Applied Physics. 123 (2018) 185301. https://doi.org/10.1063/1.5023578.

[22] H. Zschiesche, C. Alfonso, A. Charaï, D. Mangelinck, Effect of a Ti diffusion barrier on the cobalt silicide formation: solid solution, segregation and reactive diffusion, Acta Materialia. 204 (2021) 116504. https://doi.org/10.1016/j.actamat.2020.116504.

[23] D. Mangelinck, F. Panciera, K. Hoummada, M. El Kousseifi, C. Perrin, M. Descoins, A. Portavoce, Atom probe tomography for advanced metallization, Microelectronic Engineering. 120 (2014) 19–33. https://doi.org/10.1016/j.mee.2013.12.018.

[24] P. Bas, A. Bostel, B. Deconihout, D. Blavette, A general protocol for the reconstruction of 3D atom probe data, Applied Surface Science. 87–88 (1995) 298–304. https://doi.org/10.1016/0169-4332(94)00561-3.

[25] D. Mangelinck, K. Hoummada, Effect of stress on the transformation of Ni2Si into NiSi, Applied Physics Letters. 92 (2008) 254101. https://doi.org/10.1063/1.2949751.

[26] M. Putero, D. Mangelinck, Effect of Pd on the Ni2Si stress relaxation during the Ni-silicide formation at low temperature, Applied Physics Letters. 101 (2012) 111910. https://doi.org/10.1063/1.4752716.

[27] B.W. Krakauer, D.N. Seidman, Absolute atomic-scale measurements of the Gibbsian interfacial excess of solute at internal interfaces, Phys. Rev. B. 48 (1993) 6724–6727. https://doi.org/10.1103/PhysRevB.48.6724.

[28] H. Zschiesche, A. Charaï, D. Mangelinck, C. Alfonso, Ti segregation at CoSi2 grain boundaries, Microelectronic Engineering. 203–204 (2019) 1–5. https://doi.org/10.1016/j.mee.2018.10.009.

[29] H. Zschiesche, A. Charai, C. Alfonso, D. Mangelinck, Methods for Gibbs triple junction excess determination: Ti segregation in CoSi2 thin film, J Mater Sci. (2020). https://doi.org/10.1007/s10853-020-04856-4.

[30] D. Mangelinck, P. Gas, A. Grob, B. Pichaud, O. Thomas, Formation of Ni silicide from Ni(Au) films on (111)Si, Journal of Applied Physics. 79 (1996) 4078–4086. https://doi.org/10.1063/1.361770.

[31] K. Hoummada, C. Perrin-Pellegrino, D. Mangelinck, Effect of Pt addition on Ni silicide formation at low temperature: Growth, redistribution, and solubility, Journal of Applied Physics. 106 (2009) 063511. https://doi.org/10.1063/1.3204948.

[32] T. Luo, D. Mangelinck, M. Descoins, M. Bertoglio, N. Mouaici, A. Hallén, C. Girardeaux, Combined effect of Pt and W alloying elements on Ni-silicide formation, Journal of Applied Physics. 123 (2018) 125301. https://doi.org/10.1063/1.5020435.

[33] J.O. Olowolafe, M.-A. Nicolet, J.W. Mayer, Influence of the nature of the Si substrate on nickel silicide formed from thin Ni films, Thin Solid Films. 38 (1976) 143–150. https://doi.org/10.1016/0040-6090(76)90221-2.

[34] P. Gas, F.M. D'Heurle, Diffusion in Silicide, in: Diffusion in Semiconductors and Non-Metallic Solids, Ed. D.L. Beke, Springer Verlag, Berlin, 1998.

[35] F. d'Heurle, C.S. Petersson, J.E.E. Baglin, S.J. La Placa, C.Y. Wong, Formation of thin films of NiSi: Metastable structure, diffusion mechanisms in intermetallic compounds, Journal of Applied Physics. 55 (1984) 4208. https://doi.org/10.1063/1.333021.

[36] K. De Keyser, C. Van Bockstael, R.L. Van Meirhaeghe, C. Detavernier, E. Verleysen, H. Bender, W. Vandervorst, J. Jordan-Sweet, C. Lavoie, Phase formation and thermal stability of ultrathin nickel-silicides on Si(100), Applied Physics Letters. 96 (2010) 173503. https://doi.org/10.1063/1.3384997.

[37] M. El Kousseifi, K. Hoummada, T. Epicier, D. Mangelinck, Direct observation of NiSi lateral growth at the epitaxial θ-Ni2Si/Si(1 0 0) interface, Acta Materialia. 99 (2015) 1–6. https://doi.org/10.1016/j.actamat.2015.07.062.

[38] O. Cojocaru-Mirédin, D. Mangelinck, K. Hoummada, E. Cadel, D. Blavette, B. Deconihout, C. Perrin-Pellegrino, Snowplow effect and reactive diffusion in the Pt doped Ni–Si system, Scripta Materialia. 57 (2007) 373–376. https://doi.org/10.1016/j.scriptamat.2007.05.007.

[39] D. Mangelinck, K. Hoummada, F. Panciera, M. El Kousseifi, I. Blum, M. Descoins, M. Bertoglio, A. Portavoce, C. Perrin, M. Putero, Progress in the understanding of Ni silicide formation for advanced MOS structures, Physica Status Solidi A-Applications and Materials Science. 211 (2014) 152–165. https://doi.org/10.1002/pssa.201300167.

[40] J. Demeulemeester, D. Smeets, C. Van Bockstael, C. Detavernier, C.M. Comrie, N.P. Barradas, A. Vieira, A. Vantomme, Pt redistribution during Ni(Pt) silicide formation, Applied Physics Letters. 93 (2008) 261912. https://doi.org/10.1063/1.3058719.

[41] A. Schrauwen, J. Demeulemeester, A. Kumar, W. Vandervorst, C.M. Comrie, C. Detavernier, K. Temst, A. Vantomme, On the nucleation of PdSi and NiSi2 during the ternary Ni(Pd)/Si(100) reaction, Journal of Applied Physics. 114 (2013) 063518. https://doi.org/10.1063/1.4818333.

[42] W. Wopersnow, K. Schubert, Nickel-palladium-germanium alloys, Journal of the Less Common Metals. 52 (1977) 1–12. https://doi.org/10.1016/0022-5088(77)90230-2.

[43] F.M. d'Heurle, P. Gas, J. Philibert, Diffusion - Reaction: The Ordered Cu3Au Rule and Its Corollaries, Solid State Phenomena. (1995). https://doi.org/10.4028/www.scientific.net/SSP.41.93.

[44] D. Mangelinck, K. Hoummada, A. Portavoce, C. Perrin, R. Daineche, M. Descoins, D.J. Larson, P.H. Clifton, Three-dimensional composition mapping of NiSi phase distribution and Pt diffusion via grain boundaries in Ni2Si, Scripta Materialia. 62 (2010) 568–571. https://doi.org/10.1016/j.scriptamat.2009.12.044.

[45] M.-A. Nicolet, S.S. Lau, Chapter 6 - Formation and Characterization of Transition-Metal Silicides, in: N.G. Einspruch, G.B. Larrabee (Eds.), VLSI Electronics Microstructure Science, Elsevier, 1983: pp. 329–464. https://doi.org/10.1016/B978-0-12-234106-9.50011-8.

[46] R.W. Cahn, P. Haasen, Physical Metallurgy, Elsevier, 1996.

[47] Z. Zhang, B. Bai, H. Peng, S. Gong, H. Guo, Effect of Ru on interdiffusion dynamics of β-NiAl/DD6 system: A combined experimental and first-principles studies, Materials & Design. 88 (2015) 667–674. https://doi.org/10.1016/j.matdes.2015.09.041.

[48] M. Bai, H. Jiang, Y. Chen, Y. Chen, C. Grovenor, X. Zhao, P. Xiao, Migration of sulphur in thermal barrier coatings during heat treatment, Materials & Design. 97 (2016) 364–371. https://doi.org/10.1016/j.matdes.2016.02.109.

[49] M.-A. Nicolet, Diffusion barriers in thin films, Thin Solid Films. 52 (1978) 415–443. https://doi.org/10.1016/0040-6090(78)90184-0.

[50] A. Kaloyeros, E. Eisenbraun, Ultrathin Diffusion Barriers Liners for Gigascale Copper Metallization, Annual Review of Materials Science - ANNU REV MATER SCI. 30 (2000) 363–385. https://doi.org/10.1146/annurev.matsci.30.1.363.

[51] R.T. Tung, Oxide mediated epitaxy of CoSi2 on silicon, Appl. Phys. Lett. 68 (1996) 3461–3463. https://doi.org/10.1063/1.115793.

[52] S. Ohmi, R.T. Tung, Oxide Mediated Epitaxial Growth of CoSi2 in a Single Deposition Step, MRS Online Proceedings Library (OPL). 564 (1999). https://doi.org/10.1557/PROC-564-117.

[53] C. Detavernier, C. Lavoie, Texture of silicide films on Si(001) : the occurrence of axiotaxy in cubic CoSi2, tetragonal alpha-FeSi2 and orthorhombic NiSi, 2004.